Energy cascade in internal wave attractors

Thierry Dauxois[1], C. Brouzet[1], E. Ermanyuk[1,2], S. Joubaud[1], H. Scolan[1], I. Sibgatullin[1,3]

1. Univ Lyon, ENS de Lyon, Univ Claude Bernard Lyon 1, CNRS, Laboratoire de Physique, F-69342 Lyon, France
2. Lavrentyev Institute of Hydrodynamics, Novosibirsk, Russia
3. Institute of Mechanics, Moscow State University, Russia

Thierry.Dauxois@ens-lyon.fr

Abstract

One of the pivotal questions in the dynamics of the oceans is related to the cascade of mechanical energy in the abyss and its contribution to mixing. Here, we propose a unique self-consistent experimental and numerical set up that models a cascade of triadic interactions transferring energy from large-scale monochromatic input to multi-scale internal wave motion. We also provide, for the first time, explicit evidence of a wave turbulence framework for internal waves. Finally, we show how beyond this regime, we have a clear transition to a cascade of small-scale overturning events which induce mixing.

1 Introduction

The continuous energy input to the ocean interior comes from the interaction of global tides with the bottom topography yielding a global rate of energy conversion to internal tides of the order of 1TW. The subsequent mechanical energy cascade to small-scale internal-wave motion and mixing is a subject of active debate in view of the important role played by abyssal mixing in existing models of ocean dynamics. The oceanographic data support the important role of internal waves in mixing, at least locally: increased rates of diapycnal mixing are reported in the bulk of abyssal regions over rough topography in contrast to regions with smooth bottom topography. A question remains: how does energy injected through internal waves at large vertical scales induce the mixing of the fluid?

Let us consider a stratified fluid with an initially constant buoyancy frequency $N = [(-g/\bar{\rho})(\mathrm{d}\rho/\mathrm{d}z)]^{1/2}$, where $\rho(z)$ is the density distribution over the vertical coordinate z, and g the gravity acceleration. The dispersion relation is $\theta = \arcsin(\Omega)$. Here θ is the slope of the wave beam to the horizontal, and Ω (resp. $\omega = \Omega N$) is the non-dimensional (resp. dimensional) frequency of oscillations. The anisotropic dispersion relation requires preservation of the slope of the internal wave beam upon reflection at a rigid boundary. In the case of a sloping boundary, this property gives a purely geometric reason for a strong variation of the width of internal wave beams (focusing or defocusing) upon reflection. Internal wave focusing provides a necessary condition for large shear and overturning, as well as shear and bottom layer instabilities at slopes.

In a confined fluid domain, focusing usually prevails, leading to a concentration of wave energy on a closed loop, the internal wave attractor [1]. At the level of linear mechanisms, the width of the attractor branches is set by the competition between geometric focusing and viscous broadening. High concentration of energy at attractors make them prone to triadic resonance instability which sets in as the energy injected into the system increases [2]. Note that the particular case for which both unstable secondary waves have a frequency equal to half of the forcing frequency is of particular interest in the

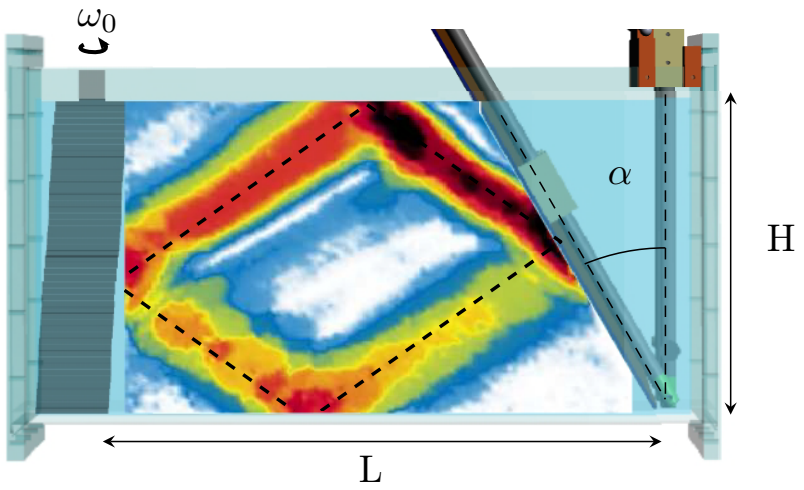

Figure 1: *Experimental set-up.* The wave generator is on the left and the inclined slope on the right. The color inset is a typical PIV snapshot showing the magnitude of the experimental two-dimensional velocity field obtained after 15 periods $T_0 = 2\pi/(N\Omega_0)$. Black dashed lines show the billiard geometric prediction of the attractor.

oceanographic context where viscosity is negligible. In that case, the appropriate name is parametric subharmonic instability and abbreviated as PSI. By abuse of language, some authors have sometimes extended the use of the name PSI to cases for which secondary waves are not corresponding to half of the forcing frequency. For the sake of terminological consistency, we propose to abbreviate triadic resonance instability using the new acronym: TRI.

The onset of instability in this case is similar to the classic concept of triadic resonance, which is best studied for the idealized case, with monochromatic in time and space carrier wave as a basic state which feeds two secondary waves via nonlinear resonant interactions. The resonance occurs when temporal and spatial conditions are satisfied: $\Omega_1 + \Omega_2 = \Omega_0$ and $\overrightarrow{k_1} + \overrightarrow{k_2} = \overrightarrow{k_0}$, where $\overrightarrow{k}$ is the wave vector while subscripts 0, 1 and 2 refer to the primary, and two secondary waves, respectively. In a wave attractor, the wave beams serve as a primary wave, and the resonance conditions are satisfied with good accuracy [2], providing a consistent physical framework for the short-term behavior of the instability.

2 The energy cascade revealed by the time-frequency diagram and the bicoherence plot

Using laboratory experiments and numerical simulations, we have shown that the set-up, sketched in Fig. 1, provides an excellent energy cascade, emphasizing how internal wave attractors can be a novel laboratory model of a natural cascade.

Indeed, the internal wave attractor is the first step: the focalisation mechanism enhances the development of the triadic instability within the beams of the attractor. While the attractor is still visible, branches are progressively deformed by triadic resonance instability, leading to the presence of secondary waves. Once the instability is well-developed, secondary waves are acting as primary waves for higher-order triadic interactions. If the focalisation is strong enough, this mechanism will of course repeat through the instability of the secondary waves. This is what is revealed by the time frequency diagram shown in Fig. 2(a). Initially, only a signal around $\Omega_0 = 0.61$ is present, but almost immediately

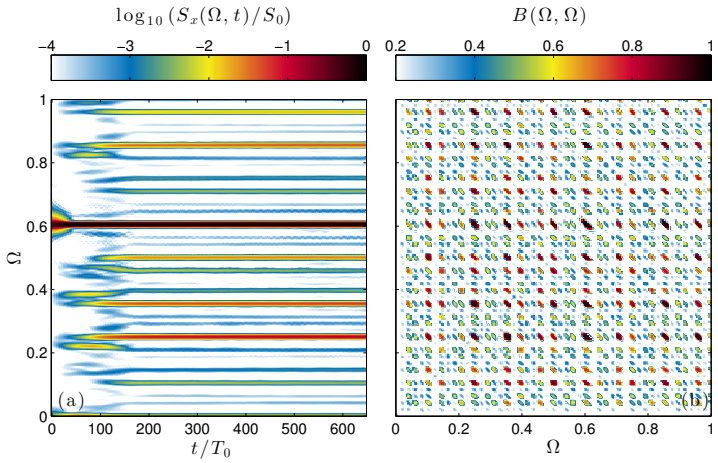

Figure 2: *Cascade of Triadic Resonance Instabilities (TRI).* Time-frequency diagram (a) and its associated bicoherence (b) of the PIV signal measures in the entire trapezoidal domain.

one distinguishes two secondary waves $\Omega_1 = 0.36$ and $\Omega_2 = 0.25$ whose sum gives Ω_0. However, again Ω_1 and Ω_2 are destabilized and this mechanism is pursued.

To detect the frequency triplets, we use the bispectrum analysis which measures the extent of statistical dependence among three spectral components (Ω_k, Ω_i, Ω_j) satisfying the relationship $\Omega_k = \Omega_i + \Omega_j$, with the quantity $M(\Omega_i, \Omega_j) = F(\Omega_i)F(\Omega_j)F^*(\Omega_i + \Omega_j)$, where F is the Fourier transform and $*$ denotes the complex conjugate. In practice, the bispectrum is usually normalized and considered in form of bicoherence which is 0 for triplets with random phases and 1 for triplets with perfect phase coupling. The bicoherence is shown in Fig. 2(b). In addition to the strong peak $(0.61, 0.61)$ corresponding to the forcing frequency (therefore to self-correlation), the possible triplets satisfying the definition of triadic resonance at $\Omega_k = \Omega_0$ can be found on the line with slope -1 connecting the points $(0, 0.61)$ and $(0.61, 0)$. This emphasizes that the mechanism at play is triadic. Other peaks are also visible corresponding to other choices of Ω_k revealing that the instability mechanism is repeated and leads to a cascade.

Thanks to this beautiful representation, it can therefore be attested that the energy transfer from global to small scales in attractors operates via a hierarchy of triadic interactions producing a complex internal wave field with a rich multi-peak discrete frequency spectrum embedded in a continuous spectrum of weaker magnitude.

3 A route towards wave turbulence

It is important to emphasize that the final stage is non-trivial since these phenomena are beyond the domain of pure wave-wave interactions: it corresponds to a regime usually called wave turbulence [3]. A similar situation takes place for surface waves, where the flourishing literature gives a fully consistent description of energy cascades between components of wave spectra, only in the case of weakly nonlinear processes, while experimental reality deals with cascades significantly "contaminated" by effects of a finite size fluid domain, wave breaking, wave cusps, nonlinear dispersion, viscous damping of wave-field components, etc. The very specific dispersion relation for internal waves introduces additional complications. For instance, in rotating fluids, which have a dispersion relation analogous to stratified fluids, the usefulness of the formalism of wave turbulence

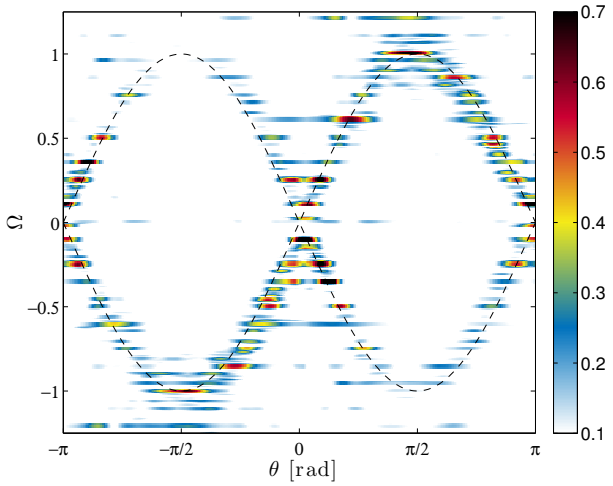

Figure 3: *Energy spectra.* Colors indicate the levels of energy spectra. The black lines correspond to the dispersion relation $\Omega = \pm \sin\theta = \pm k_x/\sqrt{k_x^2 + k_z^2}$. Integration across different wavenumbers ranges from 0.22 to 1 rad·cm^{-1}, i.e. wave lengths 28.5 cm to 6.3 cm.

as a basis for the studies in rotating turbulence has been reported for experiments only recently [4]. For internal waves, the question is still fully open, from both experimental and numerical points of view.

The presence of wave turbulence-like phenomena is illustrated in Fig. 3 using the energy spectra experimentally obtained for large scales as a diagnostic tool [4]. Horizontal and vertical velocity fields $u(x, z, t)$ and $w(x, z, t)$ are obtained with 2D PIV measurements in the entire trapezoidal domain. A two dimensions for space and one for time Fourier transform of these fields leads to $\hat{u}(k_x, k_z, \Omega)$ and $\hat{w}(k_x, k_z, \Omega)$. One can thus define the 2D energy spectrum by

$$E(k_x, k_z, \Omega) = \frac{|\hat{u}(k_x, k_z, \Omega)|^2 + |\hat{w}(k_x, k_z, \Omega)|^2}{2ST}, \tag{1}$$

where S is the area of the PIV measurement and T its duration.

In the dispersion relation for internal waves, $\Omega = \pm \sin\theta$, the wave vector $\overrightarrow{k}$ and its components do not appear directly but they are linked with the angle θ by $\sin\theta = \pm k_x/\sqrt{k_x^2 + k_z^2}$. To compute the energy spectrum as a function of variable θ, one can interpolate the energy spectrum $E(k_x, k_z, \Omega)$ to get $E(k, \theta, \Omega)$, where k is the norm of the wave vector. For this interpolation, we define Δk as the smallest wave vector that has data points in the Cartesian coordinates. Then, one can integrate over the entire range of wave vectors $[k_{min}, k_{max}]$ as follows

$$E(\theta, \Omega) = \int_{k_{min}}^{k_{max}} E(k, \theta, \Omega) k \mathrm{d}k, \tag{2}$$

or on any range of wave vectors between k_{min} and k_{max}. This is what has been done in Fig. 3 and the integration range represents 84% of the energy in the entire range $[k_{min}, k_{max}]$. The linear dispersion relation is seen to attract the maxima of the energy spectra. Above results are convincing signatures of a discrete wave turbulence framework for internal waves in this intermediate forcing amplitude regime.

If we repeat the same experiment with a larger amplitude, we have indications that a system is beyond the wave turbulence-like regime and has reached a mixing regime.

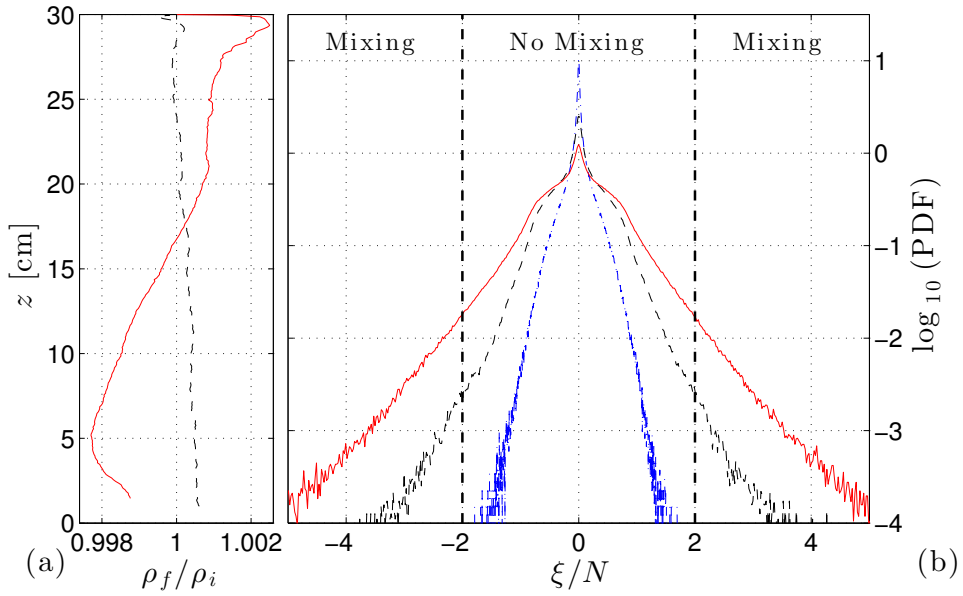

Figure 4: *Mixing and vorticity.* (a) Ratio between the density profiles measured after and before the experiments for cases with intermediate (black) and large (red) forcing amplitudes. (b) Experimental probability density functions of the vorticity, calculated on the grid from experimental images for low (blue), intermediate (black) and large (red) forcing amplitudes. Figures 2 and 3 correspond to the intermediate forcing amplitude.

Indeed, short-scale perturbations in particular clearly escape any relation to linear wave dynamics. This is expected to be due to overturnings, natural precursors to mixing.

4 Mixing inferred from vorticity distribution

An important issue is whether or not sufficiently energetic internal wave motion can produce an irreversible energy contribution to mixing. Figure 4(a) presents the comparison between density profiles measured before and after experiments: while no modification of the density (within experimental error) can be observed for the intermediate amplitude forcing that leads to wave turbulence regime described in the previous section, one gets a clear evidence of mixing in case of a larger forcing amplitude.

Further, differences between the regimes corresponding to low and high mixing are clearly seen in statistics of extreme events. This statistics is obtained by the calculation of probability density functions (PDF). Since we are interested in small-scale events destabilizing the stratification, we take the horizontal y-component of vorticity $\xi(x,z,t) = \partial u/\partial z - \partial w/\partial x$ measured in the vertical midplane of the test tank as a relevant quantity and consider the PDF of the dimensionless quantity ξ/N. In Fig. 4(b), we present the vorticity PDFs corresponding to different wave regimes in the attractor. In a stable attractor (see blue curve), extreme events are completely absent and the wave motion is concentrated within the relatively narrow branches of the attractor while the rest of the fluid is quiescent. Accordingly, the PDF has a sharp peak at zero vorticity and is fully localized between well-defined maximum and minimum values of vorticity. For larger forcing amplitudes (black and red curves), the development of TRI increases the probability of extreme events due to summation of primary and secondary wave components.

The occurrence of local overturning events can be viewed as a competition between strat-

ification and vorticity. In a two-dimensional flow, a relevant stability parameter is a version of the Richardson number, which can be introduced as $\mathrm{Ri}_\xi = N^2/\xi^2$. For a horizontal stratified shear flow this parameter reduces to the conventional gradient Richardson number $\mathrm{Ri} = N^2/(\mathrm{d}u/\mathrm{d}z)^2$, where $\mathrm{d}u/\mathrm{d}z$ is the velocity shear. Flows with large Ri are generally stable, and the turbulence is suppressed by the stratification. The classic Miles-Howard necessary condition for instability requires that $\mathrm{Ri}<1/4$ somewhere in the flow. If this condition is satisfied, the destabilizing effect of shear overcomes the effect of stratification, and some mixing occurs as a result of overturning. The threshold value $|\xi/N| = 2$ is marked on the plot of vorticity PDFs. It can be seen that data corresponding to large forcing amplitudes have "tails" extending into the domains $|\xi/N| > 2$. The area under the tails represents the probability of event of strength $|\xi/N| > 2$. In the larger forcing case (red curve), this probability is an order of magnitude greater than in intermediate one (blue curve), in qualitative agreement with the much higher mixing that has been reported.

5 Conclusion

We report and describe a novel experimental and numerical set up, an "internal wave mixing box", which presents a complete cascade of triadic interactions transferring energy from large-scale monochromatic input to multi-scale internal wave motion, and subsequent cascade to mixing. We report interesting signatures of discrete wave turbulence in a stratified idealized fluid problem. Moreover, we show how statistics of extreme vorticity events leads to mixing that occur in the bulk of the fluid.

References

[1] L.R.M. Maas, D. Benielli, J. Sommeria, F.P.A. Lam, Nature 388, 557-561, 1997. *Observations of an internal wave attractor in a confined stably stratified fluid.*

[2] H. Scolan, E.V. Ermanyuk, T. Dauxois, Physical Review Letters 110, 234501 (2013). *Nonlinear fate of internal waves attractors.*

[3] S.V. Nazarenko 2011. *Wave Turbulence.* Lecture Notes in Physics, Springer; Berlin.

[4] E. Yarom, E. Sharon, Nature Physics 10, 510-514 (2014). *Experimental observation of steady inertial wave turbulence in deep rotating flows.*

[5] C. Brouzet, E.V. Ermanyuk, S. Joubaud, I. Sibgatullin, T. Dauxois, Europhysics Letters 113, 44001 (2016). *Energy cascade in internal wave attractors.*

[6] C. Brouzet, I. Sibgatullin, H. Scolan, E.V. Ermanyuk, T. Dauxois, Journal of Fluid Mechanics 793, 109-131 (2016). *Internal wave attractors examined using laboratory experiments and 3D numerical simulations.*